# Science
**AAAS**

# Supplementary Materials for

## Proteasome-mediated protein degradation resets the cell division cycle and triggers ESCRT-III-mediated cytokinesis in an archaeon.

Gabriel Tarrason Risa, Fredrik Hurtig, Sian Bray, Anne E. Hafner, Lena Harker-Kirschneck, Peter Faull, Colin Davis, Dimitra Papatziamou, Delyan R. Mutavchiev, Catherine Fan, Leticia Meneguello, Andre Arashiro Pulschen, Gautam Dey, Siân Culley, Mairi Kilkenny, Diorge P. Souza, Luca Pellegrini, Robertus A. M. de Bruin, Ricardo Henriques, Ambrosius P Snijders, Anđela Šarić, Ann-Christin Lindås, Nick Robinson and Buzz Baum

Correspondence to: b.baum@ucl.ac.uk; n.robinson2@lancaster.ac.uk

**This PDF file includes:**

      Materials and Methods
      Figs. S1 to S14
      Tables S1 to S5
      Captions for Movies S1 to S2

**Other Supplementary Materials for this manuscript include the following:**

      Movies S1 to S2

**Methods**

**Strains, culture media and growth conditions**

The *S. acidocaldarius* strain DSM639 (WT)(DSMZ), MW001-CdvB2 (MW001 with the CdvB2 overexpression plasmid), and MW001-PAN-WkB-HA (MW001 with the PAN-WkB-HA overexpression plasmid) were grown at 75°C, pH 3.0-3.5, in Brock medium supplemented with 0.1% w/v NZ-amine and 0.2% w/v Sucrose *(35)*. The mutant *S. acidocaldarius* strains MW001 (uracil auxotroph, genetic backbone) and STK (the thymidine kinase mutant) were grown at 75°C, pH 3.0-3.5, in Brock medium supplemented with 0.1% w/v NZ-amine and 0.2% w/v Sucrose and 4 µg/ml Uracil *(24, 36)*. The optical density of liquid cell cultures was maintained at levels corresponding to exponential growth, OD600 values between 0.050 and 0.300, for between 2-12 days prior to experiments and samples were only taken within this range.

**Synchronisation and drug administration**

*S. acidocaldarius* cultures were arrested by treatment with acetic acid (final concentration 3mM) for 4.5 hours, approximately 1.5 times the doubling time *(27)*. For *in vivo* experiments the proteasome inhibitor bortezomib was added to cells at a final concentration of 10uM, EdU to a final concentration of 200 µM, and MG132 to a final concentration of 100uM. All drugs were dissolved in DMSO and equal volumes of DMSO were used as control throughout.

**Protein extraction**

25 ml *S. acidocaldarius* pellets were lysed in 100-250 µl lysis buffer (TK150 buffer, supplemented with DNAse1, and EDTA-free protease inhibitor cocktail, 0.1% Triton X-100). Cells were disrupted in a cup sonicator. After clarification, protein concentration was measured using a Bradford assay (Bio-Rad).

**RNA extraction**

TRIzol Reagent (Invitrogen) was used to isolate total RNA from 25 mL *S. acidocaldarius* pellets. The ThermoFisher trizol-reagent protocol was used for extraction. A sample clean-up was used to remove residual contaminants in which 3M $Na_4OAc$ (1:10) and 100% ethanol (5:2) was added following RNA extraction. Samples were then incubated overnight at -20°C before washed with 75% ethanol, and spun down at 12,000 rcf at 4°C for 5 minutes. Samples were resuspended in 100µl autoclaved double-distilled water. RNA concentration and purity was measured with a NanoDrop spectrophotometer. Only samples in which the 260/280 and 260/230 absorbance ratios were approximately 2.0 were used for analysis.

**Quantitative reverse transcription PCR (RT-qPCR)**

The abundance of mRNA for selected genes was measured by RT-qPCR. For each reaction, 80 ng of RNA was combined with a Euroscript reverse transcriptase (Eurogentec), 2x MESA BLUE PCR reaction mix (Eurogentec) and the primer pair (Table S5) for each gene, to reach a final volume of 14 µl. Each reaction was run in triplicate and each experiment was run in three biological replicates.

RT-qPCR was run on a Bio-Rad CFX Connect Real-Time System. Each run has 39 cycles of denaturation at 95°C for 3 seconds, annealing and extension of primers at 60°C for 45 seconds, followed by measurement of fluorescence intensity. The relative fold difference RNA abundance of each gene relative to the reference gene was derived using the $2^{-\Delta\Delta C(T)}$ method for data normalisation, with equations:

$\Delta C(T) = C(T)_{\_GENE} - C(T)_{\_REFERENCE\ GENE}$

$FD = 2^{(-\Delta C(T))}$

C(T) indicates the number of PCR cycles required to reach a threshold in fluorescence intensity of the sample. C(T) is collected for the gene of interest and reference housekeeping gene, SecY (Saci_0574) as the average of three replicates.

**ELISA**

Antibody specificity was measured using 96-well Corning Costar high-binding assay plates. Plates were coated overnight at RT with 10 µg/ml bait protein and thereafter blocked for 2 hours in PBS supplemented with 1% BSA before being incubated with primary antibodies in PBST (PBS + 0.2% Tween20) for 1 hour. Secondary antibodies conjugated with HRP (ThermoFisher) were diluted according to the manufacturer's instructions into PBST before incubating for 1 hour. 1-Step™ Ultra TMB-ELISA Substrate Solution (ThermoFisher Scientific) was added for 20 minutes before being supplemented with 1 M $H_2SO_4$ to stop the reaction. Colorimetric signal was measured at 450 nm.

**Western Blotting**

Protein samples were mixed with SDS loading buffer and incubated at 99°C for 2 minutes. 8-15 µg of protein was run on NuPAGE 4-12% Bis-Tris gels (Invitrogen) at 80-120 V using MOPS running buffer. Protein was transferred to a 0.45 µm nitrocellulose membrane and stained with ponceau to visualise total protein. Blocking was done with 5% milk and PBST (PBS, 0.2% Tween20) for 1 hour. The membrane was incubated with a 5% milk-PBST mixture with primary antibodies at 4°C overnight. The membrane was washed with PBST for 15 minutes, three times, before being incubated with a 5% milk-PBST mixture with secondary antibody for 1 hour. Finally, the membrane was washed with PBST for 15 minutes, three times, before being developed using Li-COR Odyssey Infrared Imaging System. The resulting images of the blots were analysed with ImageStudioLite.

**Washing out bortezomib in acetic acid synchronised cells**

*S. acidocaldarius* cells were synchronised with acetic acid and treated with bortezomib 80 minutes after acetic acid release. After 80 minutes cells are about to divide and a 30-minute bortezomib treatment at this time leads to there being about 20-30 % of mitotic cells arrested in division. Subsequently these cells were washed twice, i.e. spun down for 6 min at 5,000rcf and resuspended in Brock media supplemented with sucrose and NZ-amine. Then, cells were incubated for 10 minutes at 75°C, before they were washed again. After this procedure the cultures were incubated at 75°C and these mitotic cells divided within 15 minutes.

**Mass spectrometry sample preparation**

Protein samples were generated by lysing cells in 8 M urea buffer. Equal 100 µg aliquots (as determined by Bradford protein quantification, BioRad) were stored at -80ºC. Proteins were precipitated overnight in ice-cold acetone then re-suspended in 0.1 M triethylammonium bicarbonate (TEAB). Disulphide bonds were reduced by addition of 0.2 M tris(2-carboxyethyl) phosphine (incubated for 1 hour at 55 ºC) and free cysteines were capped by addition of 0.4 M iodoacetamide (incubated for 30 minutes at room temperature, protected from light). Proteins were digested with 2.5 µg of trypsin (Promega, UK) overnight at 37 ºC. Digestion was halted by acidification with 0.4 % trifluoroacetic acid and peptide samples were desalted using a C18 MacroSpin column (The Nest Group Inc, USA). Peptides were eluted with 80 % acetonitrile and divided to approx. 25 µg and 75 µg amounts. Both peptide solutions were dried in a vacuum centrifuge and stored at -80 ºC until required. Nine samples (biological triplicates of three conditions) of dried peptides (25 µg per sample) were each solubilised in 0.05 M TEAB and labelled with one of nine TMT mass tagging reagents (Thermo Scientific) from a 0.2 mg TMT 10-plex kit. The tenth channel was used to label a pooled sample. TMT labels were removed from the freezer and thawed at room temperature for 20 minutes. Labels were solubilised (20 µl of anhydrous acetonitrile) then one sample was combined with one label. Labels are amine-reactive and modify the sample's lysine residues and peptide N-termini (one-hour incubation at room temperature). Peptide labelling efficiency was assessed by analysing an aliquot using a QExactive orbitrap (Thermo Scientific) mass spectrometer. All samples displayed > 98 % labelling efficiency so were immediately quenched (addition of 1 µl of 5 % hydroxylamine) to sequester unreacted excess label. Aliquots (5 µl) were removed from each quenched sample, combined in an Eppendorf tube and mixed thoroughly. After appropriate dilution, this mix was analysed using a QExactive orbitrap mass spectrometer to determine how much of each sample had to be combined to produce a multiplexed sample containing equal peptide amounts. A final multiplexed (10-plex) sample was produced and dried in a vacuum centrifuge. The 10-plex sample was desalted using a C18 MacroSpin column, peptides were eluted with 80 % acetonitrile and the sample was dried in a vacuum centrifuge. To improve peptide coverage and quantification depth, high pH reversed-phase fractionation column was employed. The dried sample was solubilised in 0.1 % trifluoroacetic acid, loaded onto the column (Pierce, UK) and eluted into nine separate fractions using nine elution

solutions of increasing acetonitrile percentage (initial fraction 5 %; final fraction 50 % acetonitrile). The elution solution contained triethylamine to maintain a high pH value. The nine eluted fractions were dried in a vacuum centrifuge.

**Mass spectrometry**

Dried peptide fractions were re-suspended in 20 $\mu$l of 0.1% trifluoroacetic acid, sonicated for 10 minutes and centrifuged at 14,000 rpm for 3 minutes at 25 °C. Each supernatant was transferred to separate glass auto-sampler vials. Single 10 µl injections were analysed using a Fusion Lumos Tribrid orbitrap mass spectrometer coupled to an UltiMate 3000 HPLC system for on-line liquid chromatographic separation. All mass spectrometry and liquid chromatography components were sourced from Thermo Scientific, USA. The sample was loaded onto a C18 trap column (Acclaim PepMap 100; 75 µM×2 cm) then transferred onto a C18 reversed-phase column (PepMap RSLC; 50 cm length, 75 µm inner diameter). Peptides were eluted with a linear gradient of 2–25 % buffer B (75 % acetonitrile, 20 % water, 0.1 % formic acid, 5 % DMSO) at a flow rate of 275 nl/min over 135 minutes followed by a second linear gradient of 25-40 % buffer B over 25 minutes. MS1 instrument settings: spectra were acquired in the orbitrap at 120,000 resolution with scan range of 350–1500 m/z; maximum injection time 50 milliseconds; AGC target value 4E5; 30 % RF lens setting; 90 second dynamic exclusion. MS2 instrument settings: precursor ions with charge states z = 2–7$^+$ were selected for MS/MS higher-energy collision-induced dissociation (HCD) fragmentation; 38 % energy; acquired in the orbitrap at 60,000 resolution; maximum injection time 105 milliseconds; AGC target value 1E5.

**Mass spectrometry data analysis**

All data were analysed with MaxQuant software version 1.6.0.13 *(37)*. Default TMT 10-plex quantification and identification settings were used. MS/MS spectra were searched against a UniProtKB *Sulfolobus acidocaldarius* protein database (downloaded January 2019 containing 2,222 sequences composed of 349 Swiss-Prot reviewed and 1,873 TrEMBL un-reviewed sequences) using the Andromeda search engine. Data were also searched against a reversed decoy of the protein database and a list of common protein contaminants. MaxQuant settings: trypsin enzyme (C-terminal cleavage of arginine and lysine residues); two missed cleavages; Carbamidomethylation of

cysteine as a fixed modification; N-terminal protein acetylation and methionine oxidation as variable modifications. All other MaxQuant parameters were maintained at default settings including a protein and peptide false discovery rate of 1 %. The MaxQuant output proteinGroups.txt file was opened in Perseus version 1.4.0.2 *(38)*. Proteins were filtered to remove proteins identified in the common contaminant list and reverse decoy database. Intensity values were log 2 transformed and filtered to include only those proteins that provided intensity values in all TMT channels. Column then row data were normalised by median subtraction. Profile, volcano and scatter plots were generated for data visualisation and interpretation.

**MCB9463 - TMT 6-plex analysis of bortezomib / wash out experiment.**

Protein samples were generated by lysing cells in 8 M urea buffer. Equal 50 µg aliquots (Bradford quantification) were submitted to the Proteomics facility. Samples were tryptically-digested for 3 hours using the iST Sample Preparation Kit (PreOmics GmbH, Germany) following the manufacturer's instructions. Eluted peptides were dried in a vacuum centrifuge and stored at -80 ºC. Six samples (biological triplicates of two conditions) of dried peptides (50 µg per sample) were solubilised in 0.05 M TEAB and labelled with one of six TMT mass tagging reagents (Thermo Scientific) from a 0.8 mg TMT 6-plex kit as described above for the TMT 10-plex kit. Labelling efficiency assessment (> 98 %), a mixing check, production of a final multiplexed (6-plex) sample, desalting and high pH fractionation were performed as described above. MS and Proteomic data analysis were also performed as described above.

**Antibody generation**

Protein polyclonal antibodies against CdvB1 were raised in chicken by Innovagen (Lund, Sweden) according to their standard protocol including IgY purification. The protein used for immunization, was expressed and purified from E. coli Rosetta (DE3) using Ni-affinity chromatography described in Methods. Peptide antibodies against the CdvB2 peptide $NH_2$-CADVNDFLRNWG-$CONH_2$ were raised in guinea pig by Innovagen (Lund, Sweden) according to their standard protocol including IgG purification.

**Immunofluorescence labelling**

Cells were fixed by stepwise addition of 4ºC absolute ethanol until the concentration reached 70% from a starting point of 30% (30% - 50% - 70%). Samples were washed and rehydrated in PBS-TA (PBS supplemented with 0.2% Tween20 and 1% bovine serum albumin) before incubation overnight at 25°C with primary antibodies. Conjugated secondary antibodies were used for detection of the target proteins (Table S3). The S-layer was stained by incubating the rehydrated sample with 200 µg/ml Concanavalin A conjugated to Alexa Fluor 647 (ThermoFisher, C21421) for 3-5 hours. DNA was visualized by the addition of 1 µg/ml Hoechst (Invitrogen Cat, H3570) to samples after final washes. EdU was labelled via Click-IT chemistry according to kit instructions (ThermoFisher, C10639).

**Microscopy**

Microscopy samples were prepared by coating LabTek chambered slides with 2% polyethyleneimine (PEI) for 30 minutes at 30ºC. Slides were then washed with distilled water, and 200 µl of stained cell suspension was added and spun down onto the slides for 30 minutes at 1000 RCF in a swing-bucket rotor. Super-resolution was achieved using the NanoJ liveSRRF package for Fiji *(27, 28, 39)*. Images were captured for 1 second in 100 x 10 µs intervals on a Nikon Ti2, 1.49NA, 100x objective (Nikon CFI Apochromat TIRF 100XC oil objective) with a Photometrics Prime 95B sCMOS camera. Illumination was provided with a CoolLED pE-4000 LED illuminator. Analysis of ring diameters and nucleoid segregation was done with the ObjectJ plugin for Fiji (sils.fnwi.uva.nl/bcb/objectj/). Data was gathered from 3 biological replicates. The iSIM *(40)*, VisiTech, and widefield microscopy was completed on a Nikon Ti, 1.45NA, 100x objective (Plan Apo λ 100x oil) with an ORCA-Flash4.0 V3 Digital CMOS or SID4Bio camera respectively.

**Flow cytometry**

Flow cytometry analysis was carried out on BD-Biosciences LSR II and BD-Biosciences Fortessa with immunostained cells going through the following lasers and filters: lasers: 355nm, 488nm, 561nm 633nm filters: 450/50UV, 525/50 Blue, 582/15 YG, 710/50 Red. Side Scatter and Forward scatter was also recorded. Analysis was carried out on FlowJo software v10.

**Protein cloning, expression, purification for antibody verification**

CdvB, CdvB1 and CdvB2 genes were amplified from genomic *S. acidocaldarius* DNA with Phusion polymerase (NEB) according to the manufacturer's instructions. The primers used in this study can be found in Table S5 and carried homologous regions to the pSUMO-YHRC plasmid (Addgene 54336). For plasmid construction the Gibson Assembly (NEB) was used according to the manufacturer's instructions. A 2000 ml culture of E. coli Rosetta (DE3) transformed with pSUMO_S1373 (CdvB), pSUMO_S0451 (CdvB1), or pSUMO_1416 (CdvB2) was cultivated in LB media supplemented with 0.1% D-glucose, 50 µg/ml Kanamycin and 34 µg/ml Chloramphenicol at 37ºC until $OD_{600}$ reached 1.5. Following 30 minutes incubation at 4ºC, expression was induced with the addition of 0.5 mM IPTG overnight. Cells were harvested and resuspended in Buffer A (50 mM Tris pH 7.5, 500 mM NaCl, 5% Glycerol) supplemented with 20 mM imidazole before being lysed on ice through sonication. The lysate was heat-inactivated at 70ºC for 20 minutes before debris was pelleted at 20,000 RCF for 45 minutes. The supernatant was loaded onto an equilibrated His GraviTrap (GE Healthcare). The loaded column was washed with 15 ml Buffer A supplemented with 20 mM imidazole before being eluted with Buffer A supplemented with 250 mM imidazole. Fractions were loaded onto a PD10 Salt Exchange Column (GE Healthcare) equilibrated with Buffer A. Protein bearing fractions were supplemented with Ulp1 and left at RT overnight to cleave the sumo-tag. Sample were added to a His GraviTrap equilibrated with Buffer A, collecting the elute. Aliquots were snap-frozen in liquid nitrogen and stored at -80ºC.

**Overexpression of PAN-WkB-HA**

For PAN-WkB-HA overexpression, a synthetic gene containing restriction sites (PciI and XhoI) flanking the *PAN* gene with a WalkerB point mutation [E237Q] (Saci_0656-WkB) was made (Thermo Scientific®) (Fig. S12A). The gene was inserted via digestion and ligation into a pSVAaraHA-stop plasmid containing an arabinose-inducible promoter and HA tag. This was done by digesting the synthetic gene construct with PciI and XhoI, and the plasmid with NcoI and XhoI, followed by ligation. Thus, we created the plasmid pSVA-araFX-PAN-WkB-HA (Fig. S13B). The plasmid was then methylated *in vivo* by transforming the plasmid constructs into *E. coli* ER1821 (New England Biolabs) *(41).*

These methylated plasmids were then used to transform MW001 competent cells and positive colonies were selected using gelrite-Brock plates, following established practice in *Sulfolobus* genetics *(36)*.

**Overexpression of CdvB2**

For CdvB2 overexpression, a synthetic gene containing restriction sites (NcoI and XhoI) flanking the *cdvB2* gene (Saci_1416) was made (Thermo Scientific®) (Fig. S13A). The gene was inserted via digestion and ligation into a plasmid (pSVAaraFX-stop) containing an arabinose-inducible promoter, following the procedure as previously reported *(42)*. Thus, we created the plasmid pSVA-araFX-CdvB2 (Fig. S13B). The plasmid was then methylated *in vivo* by transforming the plasmid constructs into *E. coli* ER1821 (New England Biolabs) *(43)*. These methylated plasmids were then used to transform MW001 competent cells and positive colonies were selected using gelrite-Brock plates, following established practice in *Sulfolobus* genetics *(36)*.

**Crystallization of the Saci0613/Saci0662ΔN 20S core proteasome**

The inactive Saci0613/Saci0662ΔN proteasome was overexpressed in *E. coli* and purified via heat treatment at 70°C in CR buffer (100 mM Tris-HCl pH 8, 300 mM NaCl, 10% glycerol). Stable proteasome complexes were retrieved from the supernatant using Nickel-agarose IMAC chromatography and eluted in CR buffer supplemented with 500 mM imidazole. The complex was further purified by two subsequent rounds of size exclusion chromatography in GF buffer (150 mM NaCl, 20 mM Tris pH 8.0, 5% glycerol) using a Superdex 200 10/300 GL gel filtration column. Elution fractions corresponding to fully formed proteasomes (four stacks of homo-heptameric toroids) was then concentrated to 10 mg/ml. Crystals were grown using equal volumes of CZ buffer (25% PEG 1500, 0.1M MMT buffer pH5 [200 mM DL-malic acid, 400 mM MES, 400 mM Trizma]) and 10 mg/ml Saci0613/Saci0662ΔN complex. The initial 0.6 ml drops were equilibrated against a 70 ml well and the crystals generated were then used to seed 2 ml drops equilibrated against a 60 ml well, to increase the size and resolution of the crystals. Crystals were transferred to a drop of CZ solution supplemented with 30% glycerol and immediately snap frozen in liquid nitrogen. The 3.7 Å dataset was collected from a single crystal at SOLEIL (proxima 2 beamline) France at a wavelength of 0.9801 nm.

The data were integrated using XDS *(43)*. The space group symmetry was assigned in POINTLESS and intensities were scales in AIMLESS *(44)*. Molecular replacement and automated refinement were carried out in PHENIX *(45-47)*. Manual refinement was carried out using COOT *(48)*.

**Modelling of the Saci_0909ΔN catalytically active β-subunit**

A homology model of the active Saci_0909ΔN β subunit was generated with Modeller 9.20 *(49)* using the crystallographically determined structure of the inactive Saci_0662ΔN β subunit. To position the catalytic threonine correctly the structures of *Archaeoglobus fulgidus* (PDB ID code 1J2Q) and *Saccharomyces cerevisiae* (PDB ID code 4NNN) were also incorporated as templates. The final model was determined by its discrete optimised protein energy (DOPE) score.

**Docking of MG132 and bortezomib**

A docking model for bortezomib was generated in CovDock *(50)* using only the Saci_0909ΔN/Saci_0662ΔN pair of subunits that form the substrate binding pocket and receptor. The catalytic threonine of Saci_0909ΔN was identified for covalent attachment to the boronic acid moiety of the bortezomib proteasome inhibitor. Final models were chosen based on a combination of docking energy scores (kcal / mol) prior to the formation of the covalent bond and visual inspection to check for correspondence with the experimentally determined binding state of bortezomib in the *Saccharomyces cerevisiae* 20S proteasome (PDB ID: 2F16 and 4QVW).

***In vitro* 20S proteasome processing assays with bortezomib inhibition.**

The 20S proteasome core proteasome degradation reactions were performed as described previously *(16)*. 10 µg of the GFP, or 3xUrm1-GFP, was incubated with 30 µg 20S proteasome complex in reaction buffer (20 mM Tris acetate (pH 8.0), 100 mM NaCl, 5 mM $MnCl_2$, 10 mM MgOAc, 50 mM KOAc, 1 mM $Zn(OAc)_2$, 5% glycerol and 0.02% β-mercaptoethanol) in a 75 µl reaction volume at 63°C for 0, 60, 90, or 120 min, respectively. Bortezomib (solubilized in DMSO as a 100 mM stock) was added to the appropriate reactions at a final concentration of 50 µM, 3.3 µM, 1.7 µM

or 0.8 μM. After addition of 2X laemmli protein loading buffer, the products were then separated by SDS-PAGE, and visualized with Coomassie stain.

**_In vitro_ 20S proteasome processing assay with the bortezomib-insensitive mutant.**

The bortezomib-insensitive Saci0909V49T mutant construct was generated from the Saci0909ΔN clone by site-directed mutagenesis (QuikChange, Agilent) using the primer Saci0909ΔNV49T (GGATTACGACTGCAGGTAGCacTGCTGATTTACAATTTATATATGAAGC). Upon co-transformation with the Saci_0613 and Saci_0662ΔN plasmids in rosetta cells, the Saci_0613/Saci_0662ΔN/Saci_0909ΔNV49T bortezomib resistant proteasome was expressed and purified as described above and used under the same experimental conditions as the non-mutated 'wild-type' 20S proteasome complex.

**In vitro 20S proteasome processing assay of CdvB, with and without bortezomib**

The S. acidocaldarius CdvB protein was purified with modifications for proteasomal processing assays. The recombinant plasmid pSUMO_S1373 was transformed in E. coli Rosetta(DE3)pLysS strain (Novagen), protein expression was induced at mid-log phase by the addition of 0.4 mM IPTG, and cells were incubated for 3 hours at 37 °C. Cells were then harvested by centrifugation, resuspended in 50 mM Tris-HCl pH 7.5, 300 mM NaCl, 25 mM imidazole and 5 % (v/v) glycerol, lysed using French Press and clarified by centrifugation. The soluble fraction was loaded into a Histrap HP 1mL column (GE Healthcare) and the recombinant protein was eluted by the addition of the same buffer used for cell resuspension supplemented with 250 mM imidazole. The N-terminal His6-SUMO tag was removed incubating with Ulp1 SUMO protease overnight at 4°C. Finally, CdvB was purified by size exclusion chromatography using a Hiload 16/600 Superdex 75 pg column (GE Healthcare) equilibrated with 50 mM Tris-HCl pH 7.5, 300 mM NaCl and 5 % (v/v) glycerol. Protein content was analysed by SDS–PAGE and Imperial protein staining (Thermo Scientific) and concentration was determined using the BCA assay reaction kit (Pierce). Degradation by the 20S proteasome in vitro was conducted under the same experimental conditions as the non-mutated 'wild-type' 20S proteasome complex.

**Coarse-grained molecular dynamics simulations**

Following the notation from Yuan et al. *(51)*, we modelled a fluid, spherical membrane consisting of 48,000 particles with interaction parameters $\varepsilon_{bead-bead} = 4.34$ $k_BT$, $\xi = 4$, $\mu = 3$, and $r_{cut} = 1.12$ $\sigma$, where $\sigma$ is the membrane particle diameter which roughly corresponds to 10 nm in our simulations.

The ESCRT-III filament is simulated using the model developed by Harker-Kirschneck et al. *(31)*. The filament consists of three-beaded rigid subunits (see inset in Fig. 4B) which are connected to each other via the same set of nine strong harmonic bonds (bond strength $K = 600$ $k_BT$). Because the resting bond lengths between subunits are the same throughout the filament, they define what shape the filament will adopt when at rest. They are chosen so that the filament possesses an intrinsic 3D curvature and hence forms a ring in its rest state with target radius $R_{target}$. By varying the bond lengths, we can vary the target radius and form larger and smaller filament helices. The green beads of the filament are attracted to membrane beads at a distance $r_{ij}$ via a Lennard-Jones potential:

$E_{ij} = 4$ $\varepsilon$ $((\sigma/r_{ij})^{12}-(\sigma/r_{ij})^6)$, for $r_{ij} < r_c$, with $\varepsilon = 4$ $k_BT$, $\sigma = 10$ nm and $r_c = 11.2$ nm. The yellow filament beads only interact with the membrane via volume exclusion (meaning they can't overlap with, but are not attracted to, the membrane). Volume exclusion also applies to subunits within the filament interacting with each other.

In order to investigate how the constriction and disassembly of the ESCRT-III filament affects the cell membrane dynamics, we ran our simulations with the Molecular Dynamics package LAMMPS (https://lammps.sandia.gov/) *(52)*. All particles in the system experience Langevin dynamics with friction coefficient $\gamma = m / t_0$ set to unity, where m is the particle mass (set to unity for all particles) and $t_0$ is the simulation unit of time. The filament starts off in the the CdvB1(CdvB+) state in which it has a low curvature (large initial radius $R_0$ resembling the cell radius). We first equilibrate the system for $2 \times 10^5$ time-steps (with a fixed time-step of 0.01 $t_0$, where $t_0$ is the molecular dynamics unit of time), to ensure that the ESCRT-III filament attaches to the membrane.

We then model the state after CdvB degradation by reducing the radius of the filament by 95% ($R_{target}/R_0 = 5\%$), while keeping it attached to the membrane (entering the CdvB1(CdvB-) state). This is done by adjusting the resting bond lengths of the filament to a smaller target radius, and it happens instantaneously, meaning all bonds within the filament are adjusted at the same time.

In the simulation that includes disassembly, we then begin to disassemble the filament by removing individual subunits from both ends of the helix by turning their bond strengths to 0 (bond strength $K = 0$ $k_B T$). Every 2000 time steps two bonds are removed, making the disassembly rate $\lambda = 2/(20$ $t_0)$. Consequently, the filament length $N(t) = N_0 - \lambda t$ decreases linearly in time. For simplicity the filament length $N(t)$ is defined as the number of subunits that is still integrated in the filament at time t.

This process continues until the last subunit of the ESCRT-III filament is disassembled. After that the simulation equilibrates for another $10^6$ time-steps. In the simulation without the disassembly the filament equilibrates for $10^7$ time-steps right after the instantaneous curvature change. The simulation results are then visualized by the open-source software OVITO *(53)*.

**Stochastic sampling method for CdvB degradation**

The data suggests that rapid degradation of CdvB is key to cell division. In order to investigate how quickly the initial CdvB level is degraded in time, we use a simple stochastic sampling method. For that purpose, we assume that the CdvB level of each individual cell follows a power law with intrinsic exponent \alpha. Based on that we sample CdvB levels for an ensemble of cells that are stochastically distributed in time (i.e. an asynchronous exponentially growing population). This computational procedure agrees with the experimental measurements shown Fig S10C. Consequently, by varying the model exponent \alpha and comparing the result to experiments we can determine which \alpha best fits the experimental data and thus find how quickly CdvB is degraded prior to cell division.

A power law was assumed for how the initial CdvB level degrades over time, i.e. $L(t) = L_0 - r * t^{\alpha}$. $L_0$ is the initial CdvB level that follows a Gaussian distribution according to the data in the peak CdvB-CdvB1 population in asynchronous cell populations. The constant associated to the speed of the process, r, was assumed to be fixed for all the cells. We defined it as $r = (L_i - L_f) / (T^{\alpha})$, where it is assumed that $L_i$ is the largest value measured and $L_f$ is the smallest value measured, and T is the time that the whole process took to finish. Alpha is the exponent of the power law.

For the sampling, a random number was chosen for the initial value $L_0$ according to the Gaussian distribution and another random number for the time t at which the CdvB level in a specific cell is measured. That time is uniformly distributed over [s * lifetime;lifetime], where s< 1 indicates the start of the measurement. Lifetime = $((L_0 - L_f) / r)^{(1 / \alpha)}$ is the time it would take to degrade an initial random level $L_0$ to the final value $L_f$, please note this is an approximation given that $L_f$ is fixed for all cells. Also, please note that the measurements end before CdvB is fully degraded, i.e. lifetime is not the time to reach $L(t) = 0$ but to reach $L(t) = L_f$, and that the measurements start not at time $t = 0$ but at time $t = s * $ lifetime. This is in line with the data, as the degrading CdvB population does not reach a zero level. A cell's specific CdvB level is then estimated to be $L(t) = L_0 - r * t^{\alpha}$ and that value then stored. This process is repeated 7292 times, for as many cells as there are in the population called degrading CdvB, and the results are then sorted in descending order.

The above procedure was completed for different combinations of the parameters alpha and s and compared to the result to the experimental data. From that, $\alpha = 0.22$ and $s = 0.12$ came close to the experimental data. The fact that the scaling exponent $\alpha$ is small (substantially smaller than one) confirms that CdvB degrades quickly in the beginning of the division process to trigger constriction.

**Statistical analysis**

All statistical analysis and data processing were done using Microsoft Excel or GraphPad Prism 6 software. Significance was defined as $p < 0.05$. Significance levels used were $*P < 0.05$, $**P < 0.01$, $***P < 0.001$ and $****P < 0.0001$.

Supplementary Figure 1 Crystal structure of the *S.acidocaldarius* proteasome

**A**

Side and top-down view of the 28 subunit proteasome
(Saci_0613/Saci_0662ΔN)

α-ring
(Saci0613)

β-ring
(Saci0662ΔN)

β-ring
(Saci0662ΔN)

α-ring
(Saci0613)

140 Å

90°    90°

110 Å

**B**

Side view of the 28 subunit proteasome
with a model of the Saci0909ΔN catalytic subunit (light green)

180°

Modelled
chymotryptic/active
β-subunit
(Saci0909ΔN)

α-ring
(Saci0613)
β-ring
(Saci0662ΔN)
β-ring
(Saci0662ΔN)
α-ring
(Saci0613)

**C**

Top-down view of the alpha subunit ring
highlighting its open gate conformation

110 Å

TYR10
ALA13
ARG12

**E**

Model of bortezomib bound
to the *S. acidocaldarius*
chymotryptic/active Saci0909ΔN β-subunit
(surface view)

**D**

Side view of the 28 subunit proteasome
highlighting the catalytic site

140 Å

THR160
ASP166
ASP17
SER129
LYS33
THR1

Crystal structure of bortezomib
bound to *S. cerevisiae* chymotryptic/active
β5-subunit (PDB: 2F16)

LYS33
SER131
BORT
THR21
SER1
SER171
THR1
ASP166

**Supplementary Figure 1 Crystal structure of the S. acidocaldarius proteasome.** (**A**) (top) Side view of the S. acidocaldarius twenty-eight subunit Saci_0613/Saci_0662ΔN 20S proteasome assembly. (bottom) The 20S barrel rotated through 90° to provide a top-down view of the structure highlighting the 'open' entrance pores and the translocation channel passing through all three chambers. Saci_0613 α-subunits are coloured alternatively dark-, light-blue and the final subunit purple. Saci_0662ΔN β-subunits are coloured alternatively dark-red, light-red and the final subunit beige. (**B**) Side view of the 20S proteasome assembly, with the modelled Saci_0909ΔN catalytic subunit (light green) inserted into the Saci_0613/Saci_0662ΔN 20S crystal structure. (**C**) Top-down view of the S. acidocaldarius twenty-eight subunit Saci0613/Saci0662ΔN 20S proteasome assembly, including the modelled Saci909ΔN active subunit, highlighting the 'open' conformation of the alpha-subunit gating. The outer rings are formed from a homo- heptameric arrangement of Saci0613 alpha-subunits, which are coloured purple and then alternately marine-blue and light-blue. The Saci0662ΔN beta-subunits of the inner rings are coloured alternately dark-red, light red and the final subunit beige. The extended region of α-subunit-1 residues 6-14 (AAMGYDRAI) (highlighted by the green-dashed circle) is coloured red and the side chains of these residues are shown as sticks. (right) magnified view of the pore region, highlighting the additional residues 6-14 (AAMGYDRAI) that could be built into the density map at the N-terminus of α- subunit-1. (**D**) Side view of the 20S proteasome assembly with the extended region of α-subunit-1 residues 6-14 (AAMGYDRAI) highlighted by the green-dashed circle. Note the modelled Saci909ΔN active subunit (green) is on the opposing side of the beta-ring. (right) Magnified view through the Saci0662ΔN beta-ring, with a cutaway to reveal the modelled Saci909ΔN active subunit (green) and the key catalytic residues (Thr1, Asp17 and Lys33) at the active site, with three further conserved residues (Ser129, Asp166 and Thr169), which are thought to aid catalysis and maintain the structure of the active site. (**E**) Modelled binding of the reversible inhibitor bortezomib to the Saci_0909ΔN chymotryptic site in the S. acidocaldarius 20S proteasome, using the CovDock software. Surface view (top) of the bortezomib inhibitor (orange sticks) covalently attached to the active site threonine (Thr1), shown as a red stick covalently bound to boronic acid group of the bortezomib molecule. (bottom) Crystal structure (PDB:2F16) of bortezomib binding at the *S. cerevisiae* 20S proteasome focusing on substrate binding pocket formed between the β5 chymotryptic β-subunit (light green) and adjacent β-subunit (brown).

Supplementary Figure 2 Electron density map of the core 20S *S. acidocaldarius* proteasome

**A**
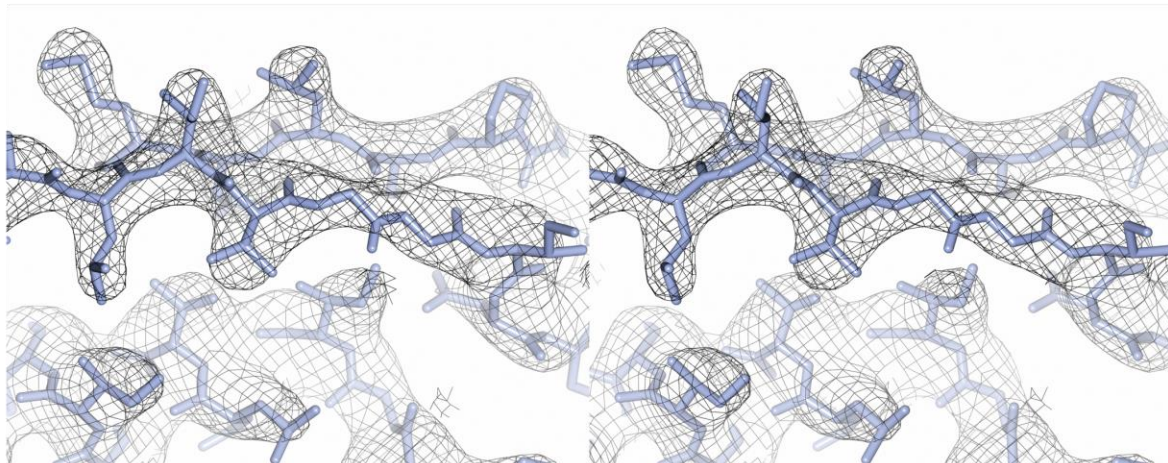


**B**
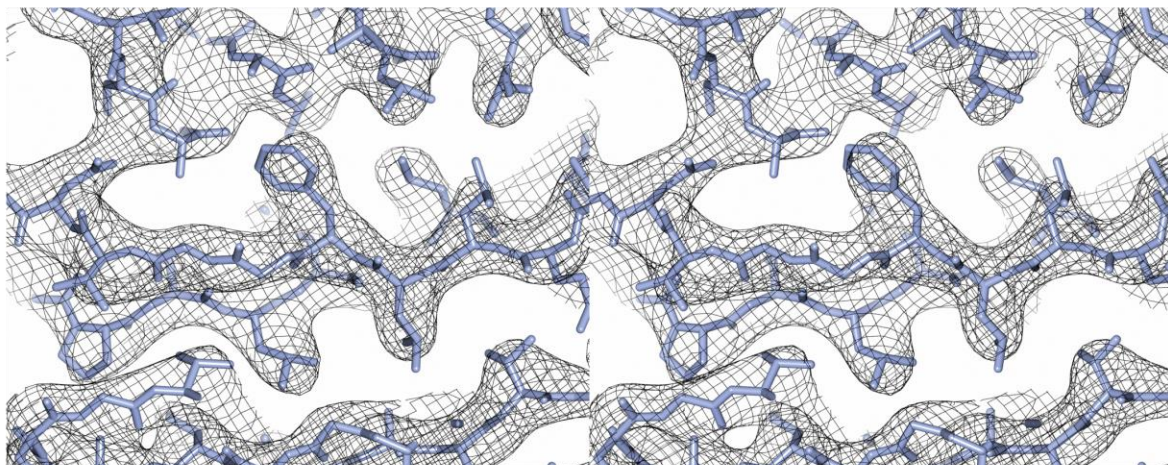


**C**



.

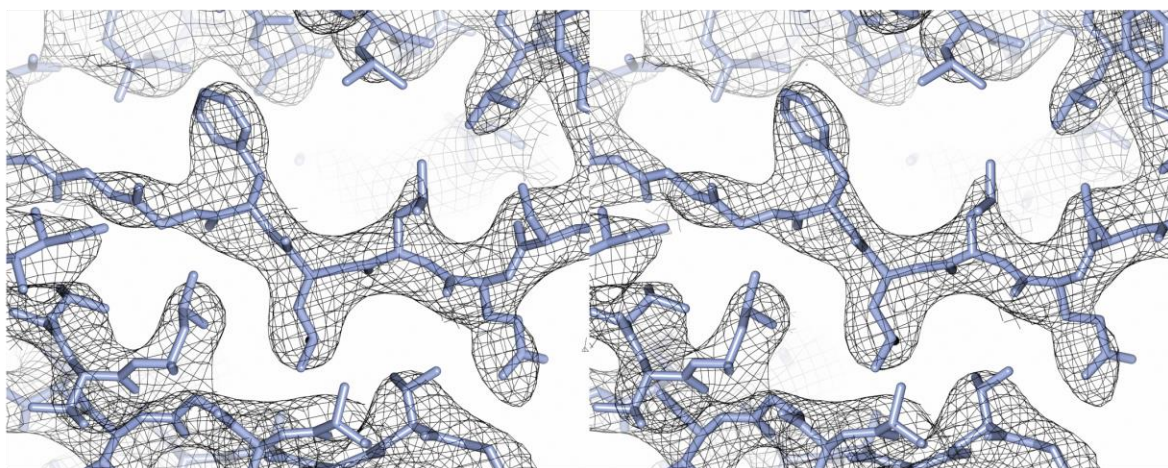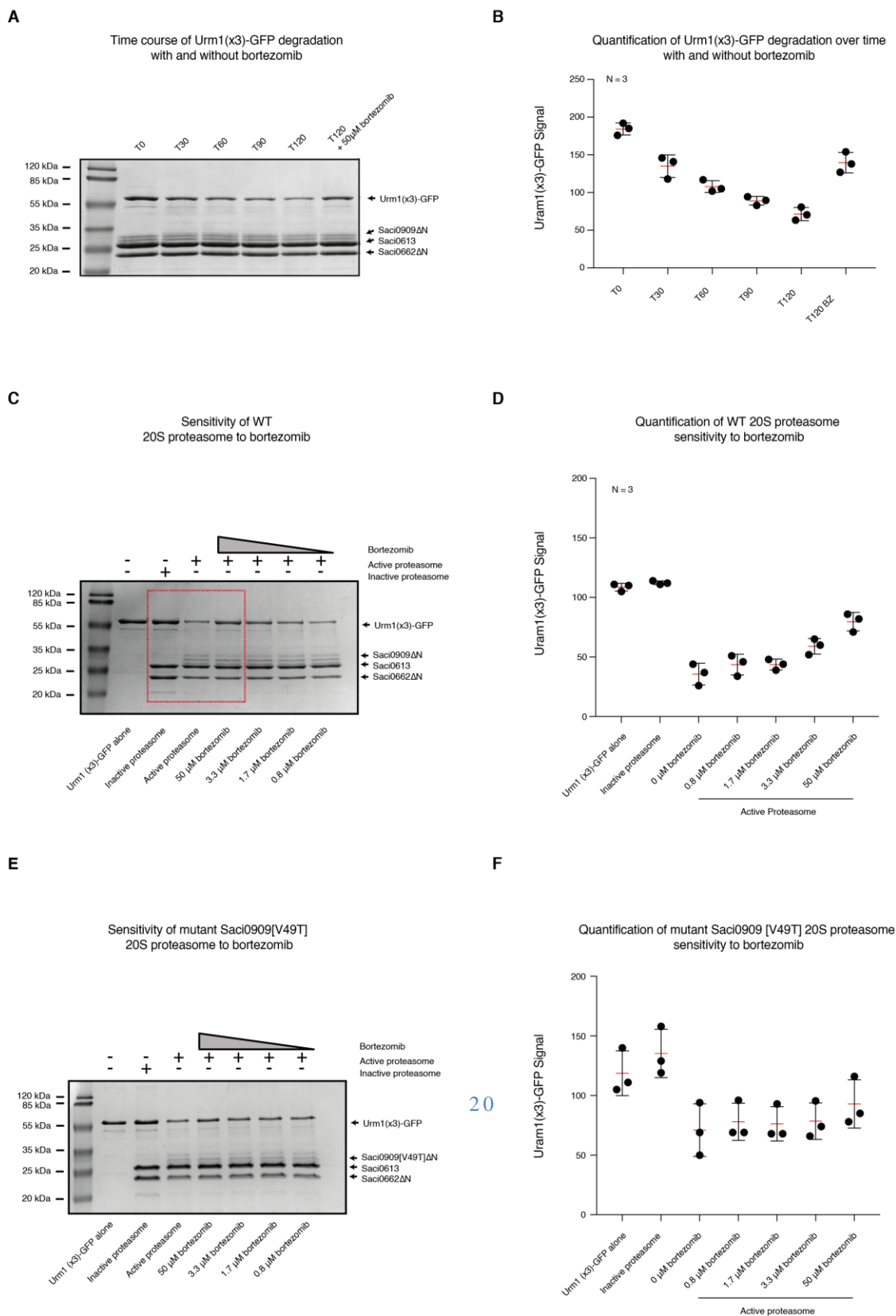**Supplementary Figure 2 Electron density map of the core 20S S. acidocaldarius proteasome.** Stereo image of a portion of the electron density map of the S. acidocaldarius Saci_0613/Saci_0662ΔN proteasome structure [Type of map: mtz, Contour level: 1 sigma]. (**A**) Segments from subunit B secondary structure element α-3. (**B**) subunit B secondary structure element β-5. (**C**) subunit a secondary structure element β-6.

# Science
### AAAS

## Supplementary Figure 3 In vitro proteasome activity and sensitivity to bortezomib

**A**

Time course of Urm1(x3)-GFP degradation
with and without bortezomib



**B**

Quantification of Urm1(x3)-GFP degradation over time
with and without bortezomib



**C**

Sensitivity of WT
20S proteasome to bortezomib



**D**

Quantification of WT 20S proteasome
sensitivity to bortezomib



**E**

Sensitivity of mutant Saci0909[V49T]
20S proteasome to bortezomib



**F**

Quantification of mutant Saci0909 [V49T] 20S proteasome
sensitivity to bortezomib



20

**Supplementary Figure 3 In vitro activity and sensitivity of the 20S S. acidocaldarius proteasome to bortezomib.** (**A**) Time course of a 20S proteasome assay with Saci_0613/Saci_0662ΔN/Saci_0909ΔN using 3xUrm1-GFP substrate. 10 µg of 3xUrm1-GFP substrate was incubated with 30 µg of the active proteasome complex for 0, 30, 60, 90 or 120 minutes at 63°C. In the last lane 3xUrm1-GFP is incubated with the 20S proteasome for 120 minutes at 63°C, but also with 50 µM bortezomib inhibitor. (**B**) Quantification of the 20S proteasome time course assay showing the degradation of Urm1(x3)-GFP signal over time. Error bars represent means ± SD from N = 3. (**C**) 20S proteasome bortezomib sensitivity assay using 3xUrm1-GFP substrate. 10 µg of 3xUrm1-GFP substrate was incubated with 30 µg of the active proteasome complex in conditions with 50 µM, 3.3 µM, 1.7 µM and 0.8 µM bortezomib at 63°C. 3xUrm1-GFP substrate degradation activity of an inactive 20S proteasome assembly made up of Saci_0613/Saci_0662ΔN was used as a negative control. The Saci_0613/Saci_0662ΔN/ Saci_0909ΔN active 20S proteasome assembly was also used in the absence of the inhibitor as a positive control. The red dashed-box region indicates the sections of the gel that are presented in Figure 1C in the main text. (**D**) Quantification of the 20S proteasome bortezomib sensitivity assay, showing Urm1(x3)-GFP degradation when incubated with different concentrations of bortezomib. Error bars represent means ± SD from N = 3. (**E**) The same experimental conditions as in (C) carried out with a mutant β active subunit Saci_0909 [V49T]. (**F**) Quantification of the mutant β active subunit Saci_0909 [V49T] mutant proteasome assembly's sensitivity to bortezomib assay, showing Urm1(x3)-GFP degradation when incubated with different concentrations of bortezomib. Error bars represent means ± SD from N = 3.

Supplementary Figure 4 Cell cycle responses to proteasomal inhibition
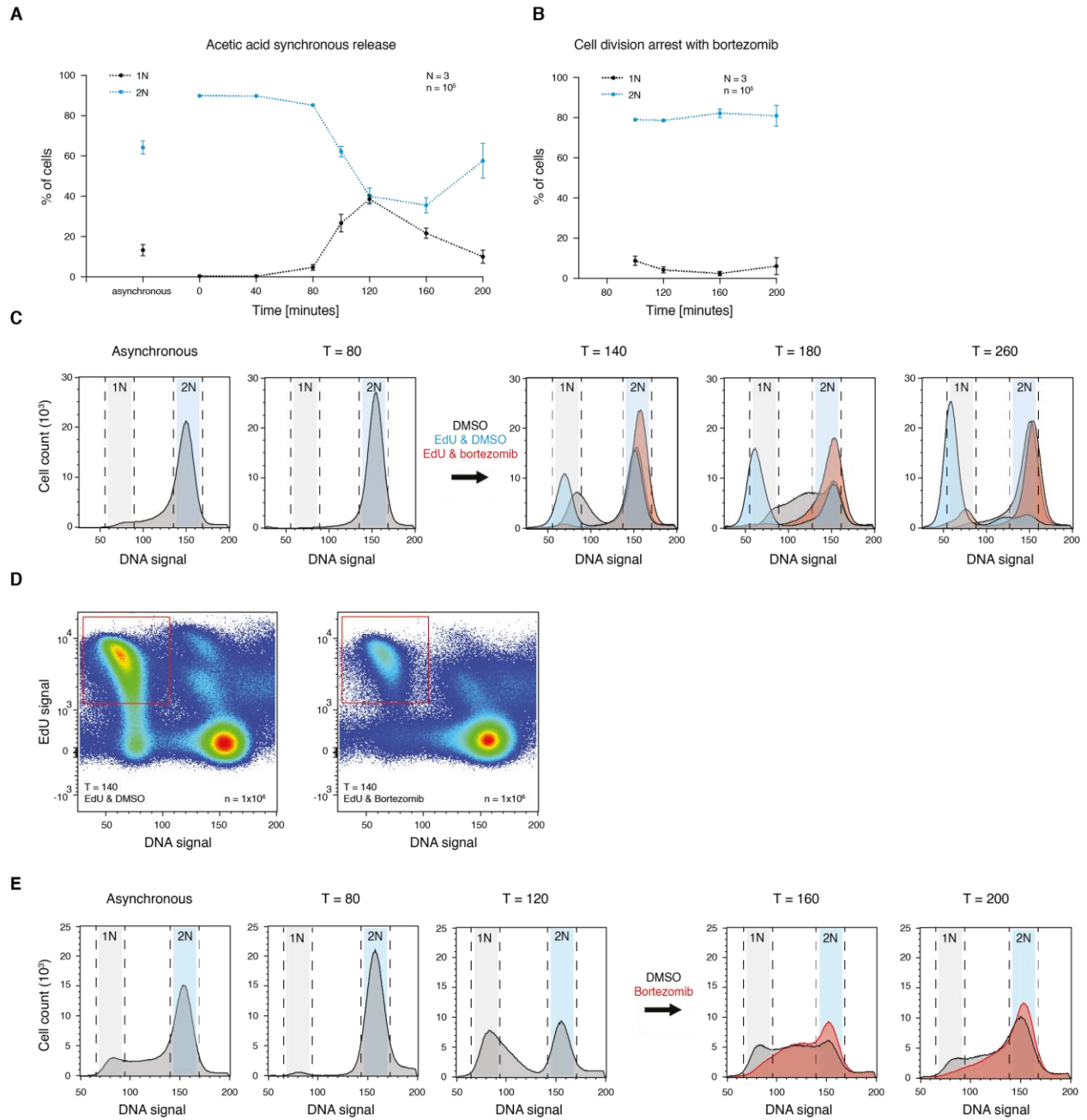
**Supplementary Figure 4 Cell cycle responses to proteasomal inhibition.** (**A**) Graph with the distribution of cells with 1N and 2N DNA content in a population following acetic acid synchronisation and release. Error bars represent means ± SD from N = 3, n = $10^5$. (**B**) Graph with the distribution of cells with 1N and 2N DNA content in a population following bortezomib treatment of synchronised pre-division cells 80 min after release. Error bars represent means ± SD from N = 3, n = $10^5$. (**C**) Flow cytometry histograms showing the number of cells with 1N and 2N DNA content in an STK population after acetic acid synchronisation and bortezomib treatment pre-division. EdU was added to the synchronised population 80 min after release from acetic acid, and bortezomib was added 100 min after release from acetic acid. N = 3, n = $10^6$. Representative histograms shown. (**D**) Flow cytometry scatterplots showing the individual cells' EdU content vs DNA content from a synchronised STK population 140 minutes after release. The cells had been treated with DMSO or bortezomib, respectively, 100 min after release. The red quadrant shows the S-phase cells with EdU incorporated. Each blue spot represents a single cell, the density gradient going from blue to red. Representative blot shown, N = 3 n = $10^6$. (**E**) Flow cytometry histograms showing the number of cells with 1N and 2N DNA content in a population following acetic acid synchronisation and bortezomib treatment 120 min after release (post-division). N = 3, n = $10^6$.

# Supplementary Figure 5 Proteasomal inhibition with MG132

**A**



**B**

Impact on the proteome upon proteasome inhibition with MG132 during cell division
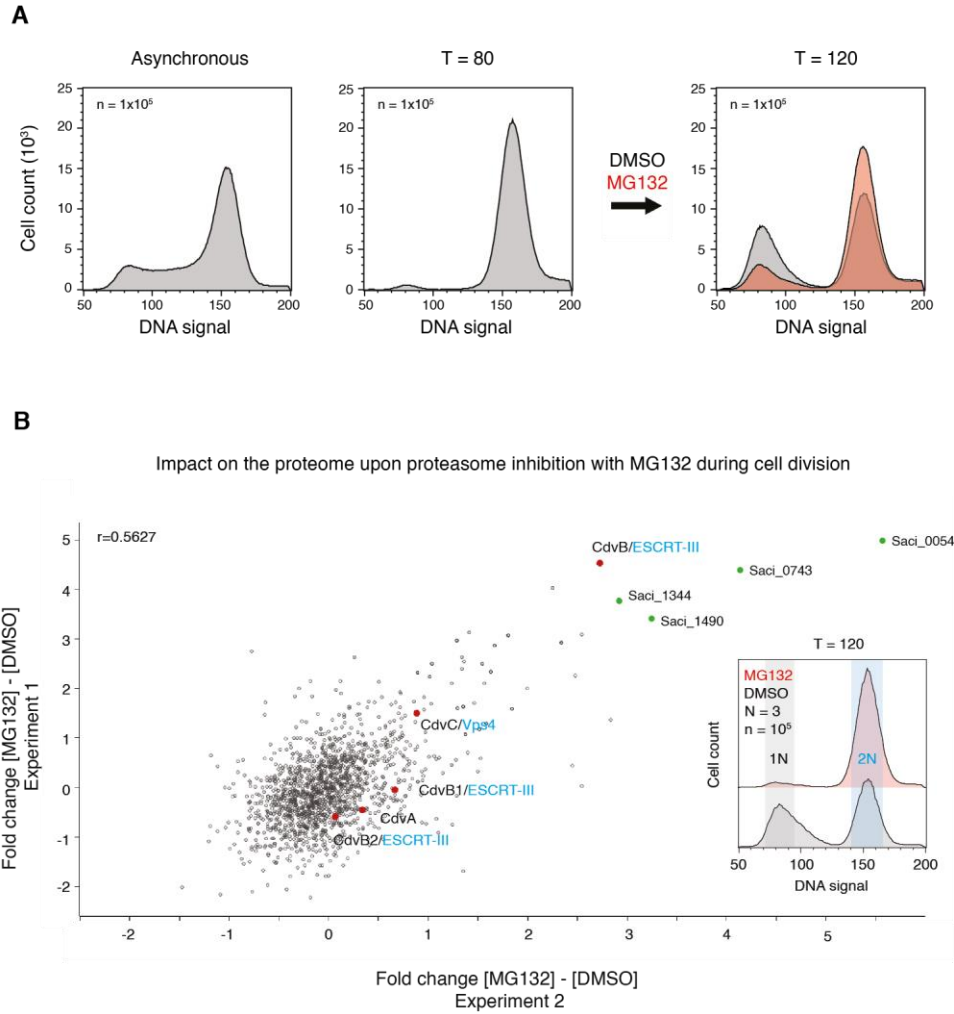
**Supplementary Figure 5 Proteasomal inhibition with MG132.** (**A**) Flow cytometry histograms showing the distribution of cells with 1N and 2N DNA content in an asynchronous population (left), a population after release from acetic acid synchronisation but prior to division (middle), and a pre-division synchronised population treated with MG132 or DMSO for 40 min. Representative histograms shown. N = 3, n = $10^5$. (**B**) Mass spectrometry scatterplot correlating two independent replicates showing the difference in proteomes of pre-division synchronised cells treated with MG132 (1) or DMSO (2) for 40 min. Protein values were measured as the ratio of TMT intensities subtracting log2 transformed values of sample (2) from sample (1). The top 5 hits are highlighted in green (except CdvB) and labelled with S. acidocaldarius gene extensions. See supplement for complete tables with the data from three independent experiments. The insert shows two representative histograms of the MG132 and DMSO treated samples.

Supplementary Figure 6 *S. acidocaldarius* ESCRT-III homologue antibody specificities
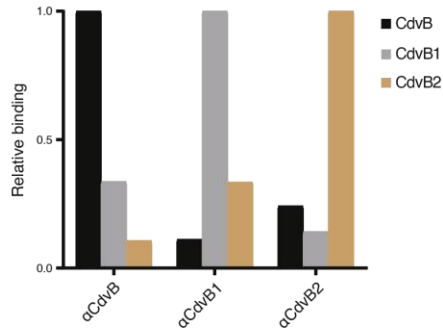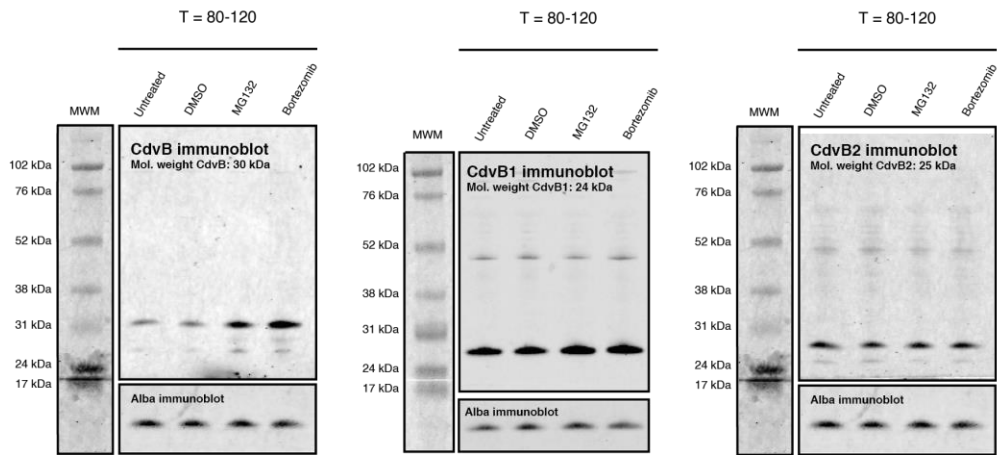
**Supplementary Figure 6 S. acidocaldarius ESCRT-III homologue antibody specificities.** (**A**) In vitro ELISA analysis of CdvB, CdvB1 and CdvB2 antibody specificities. CdvB (black), CdvB1(grey) or CdvB2 (beige) was coated onto a well before detection with antibodies, shown as αTarget. (**B**) Full western blots for synchronised cells in the presence and absence of proteasome inhibitors, probing with CdvB, CdvB1 and CdvB2 antibodies. These immunoblots show that the antibodies for CdvB, CdvB1, and CdvB2 detect proteins at the appropriate molecular weights. Cut-outs of the proteins reported here are shown again quantified in Figure S7B.

Supplementary Figure 7 cdv transcript and protein level response to proteasomal inhibition

**Supplementary Figure 7 Cdv RNA transcript and protein level response to proteasome inhibition.** (**A**) Time course showing qPCR transcript abundance of Cdv proteins in an acetic acid synchronised population treated with bortezomib or DMSO 80 min after release (pre-division). Transcript levels were normalised to *secY* (non- cyclical control gene) and plotted relative to the 'asynchronous' condition. Error bars represent means ± SD from N = 3. (**B**) Left, western blots of CdvA, CdvB, CdvC, CdvB1, and CdvB2 protein levels, with Alba as a loading control. All samples were taken 120 min after release from acetic acid synchronisation, after having been left untreated or treated with DMSO, MG132, or bortezomib for 40 minutes (i.e. from T80-120). Representative blots shown. Right, quantification of the western blots shown as fold change of protein relative to the untreated condition and normalised with Alba. Error bars represent means ± SD from N = 3.

Supplementary Figure 8 Targeted degradation of CdvB triggers constriction via CdvB1 and CdvB2
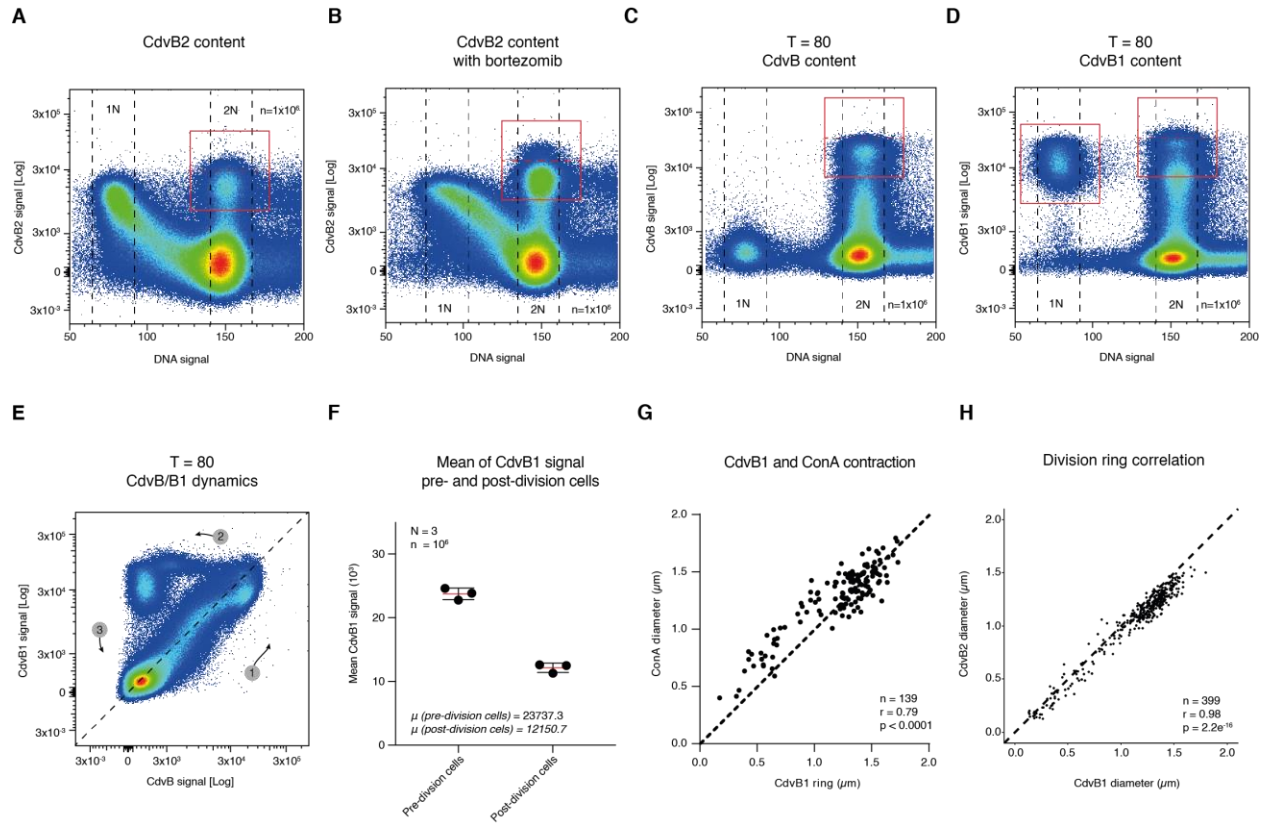
**Supplementary Figure 8 Targeted degradation of CdvB triggers constriction via CdvB1.** (**A**) Flow cytometry scatterplot with CdvB2 signal versus DNA signal for an asynchronous population. Red insert frames the "mitotic" cells with high signal. Each blue spot represents a single cell, the density gradient going from blue to red. Representative plot shown. N = 3, n = $10^6$. (**B**) Flow cytometry scatterplot with CdvB2 versus DNA signal for an asynchronous culture treated with bortezomib. Red insert frames "mitotic" cells with high signal. Each blue spot represents a single cell, the density gradient going from blue to red. Representative plot shown. N = 3, n = $10^6$. (**C and D**) Flow cytometry scatterplots with CdvB and CdvB1 signal, respectively, against DNA signal for a synchronous culture 80 min after release, in which fewer than 5% of cells have divided. The red inserts frame "pre-division" cells with high signal and in (**D**) a second red square frames the recently divided cells with 1N DNA signal and high levels of CdvB1. Each blue spot represents a single cell, the density gradient going from blue to red. Representative plots shown. N = 3, n = $10^6$. (**E)** Flow cytometry scatterplot of CdvB1 vs CdvB signal for a synchronous culture 80 min after release in which fewer than 5% of cells have divided. Note the accumulation and loss of CdvB and CdvB1 protein indicated with the numbers/arrows. Each blue spot represents a single cell, the density gradient going from blue to red. Representative plots shown. N = 3, n = $10^6$. (**F**) Quantification of CdvB1 signal in pre-division cells. Error bars represent means ± SD from N = 3, n = $10^6$. (**G**) Correlative analysis of S-layer diameter as identified by concanavalin A vs CdvB1 ring diameter from widefield micrscopy. N = 3, n = 139. (**H**) Correlative analysis of CdvB2 and CdvB1 ring diameters from SRRF super resolution microscopy. All quantifications cover more than 6 fields of view and 3 biological replicates. N = 3, n = 399.

## Supplementary Figure 9 Estimation of the timeline of cell division in *S. acidocaldarius*

**A**

CdvB1 signal vs CdvB signal
2N cells only



**B**

Mathematical relationship (binary fission) between
observed cell cycle states in an asynchronous population
and cell division cycle time

$$n(a) = 2 \cdot \ln 2 \cdot e^{-a \ln 2}$$



Cell division cycle timeline

**C**

Estimation of cell division timeline

| | B. Replicate 1 | B. Replicate 2 | B. Replicate 3 | Average | St. deviation | Binary fission adjusted % | Doubling time | Time in min | % of dividing population |
|---|---|---|---|---|---|---|---|---|---|
| High CdvB I Low CdvB1 | 0.94% | 1.10% | 1.32% | 1.12% | 0.19% | 1.58% | 165 | 2.6 | 41% |
| Peak CdvB I Peak CdvB1 | 0.75% | 0.54% | 1.06% | 0.78% | 0.26% | 1.12% | 165 | 1.8 | 29% |
| Degrading CdvB I High CdvB1 | 0.80% | 0.77% | 0.76% | 0.78% | 0.02% | 1.12% | 165 | 1.8 | 29% |
| Total diving cell population | 2.48% | 2.41% | 3.14% | 2.68% | 0.40% | 3.81% | 165 | 6.3 | 100% |

**Supplementary Figure 9 Estimation of the timeline of cell division in S. acidocaldarius. A**) Flow cytometry scatterplot of CdvB1 vs CdvB signal for an asynchronous population in which all cells with less than 2N DNA signal have been removed. Red insert: population of cells with peak CdvB and low CdvB1 signal (corresponding to cells with CdvB+ and CdvB1- rings). Yellow insert: population of cells with peak CdvB and peak CdvB1 signal (corresponding to cells with CdvB+ and CdvB1+ rings). Green insert: population of cells degrading CdvB and with peak CdvB1 signal (corresponding to cells with CdvB- and CdvB1+ rings). Each blue spot represents a single cell, the density gradient going from blue to red. Representative plot shown. N = 3, n = $10^6$. **B**) Graphical representation of the mathematical relationship between observed cell cycle states in an asynchronous population growing exponentially with binary fission and the actual cell cycle time. Note that the earliest stage of the cell cycle will be two times more frequently observed than the latest state of the cell cycle. The defined integral of function n(a) returns the observed percentage of cells with respect to the percentage covered by the cell cycle timeline (0 being the start and 1 the end of the cycle). **C**) Estimation of the cell division timeline on the basis of the CdvB and CdvB1 dynamics. Note the stability of the percentage of cells degrading CdvB and the variation in the percentage of cells with CdvB-CdvB1 rings and CdvB rings alone. Overall the process of division appears to take about 6.3 minutes and the actual cell constriction (coinciding with CdvB degradation) about 1.8 minutes. The number of cells with peak CdvB content observed by flow cytometry corresponds to the percentage of cells with rings as observed by microscopy. N = 3, n = $10^6$.

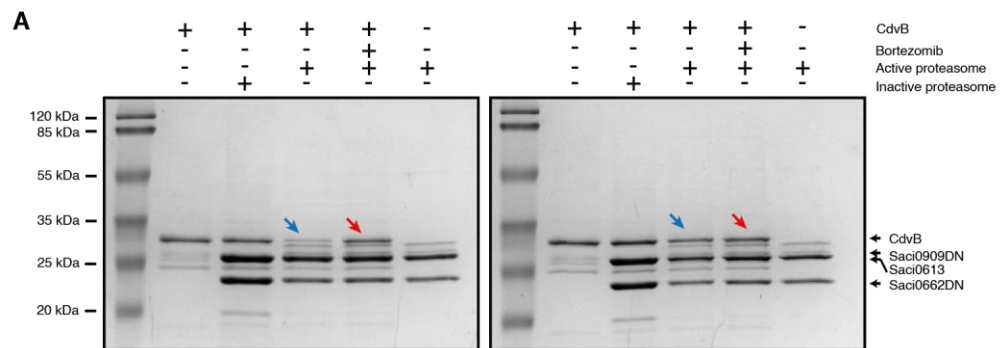Supplementary Figure 10 Degradation and disassembly dynamics of the ESCRT-III cell division ring
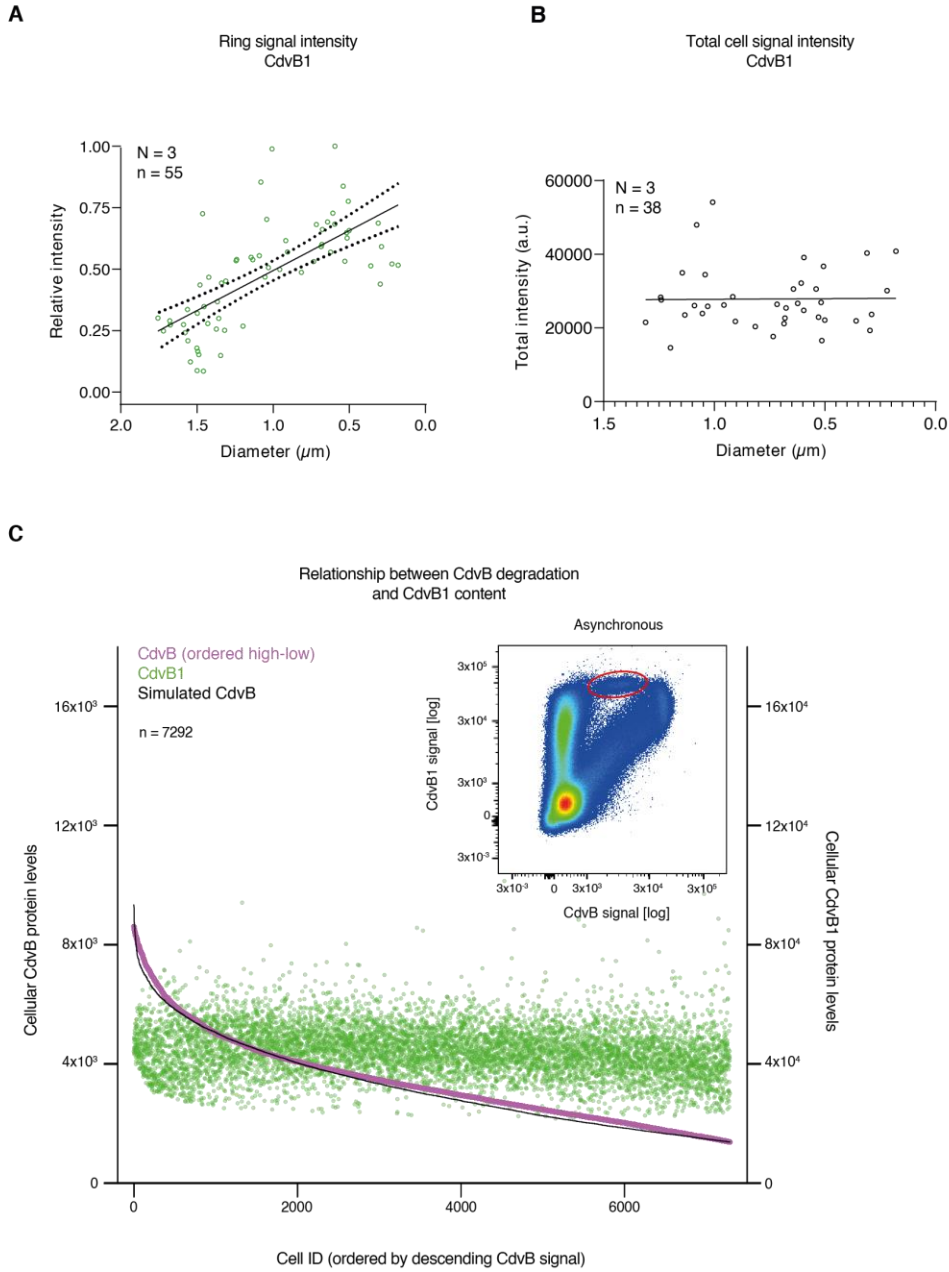
**Supplementary Figure 10 ESCRT-III dynamics during cell division. A**) Graph plotting the CdvB1 ring signal intensity as a function of its diameter. N = 3, n = 55. **B**) Graph plotting the total CdvB1 signal of a cell as a function of its diameter. N = 3, n = 38. The images studied for these datasets were obtained with iSIM (unprocessed) widefield microscopy **C**) Graph comparing CdvB protein level (purple) and CdvB1 protein level (green) present in cells that are degrading CdvB and about to divide. The CdvB curve follows a power law with exponent \alpha=0.22 reproduced with stochastic sampling in black which supports the understanding that CdvB is rapidly degraded to trigger cell division (see methods). The inset shows the CdvB1 vs CdvB signal in an asynchronous population of cells. The population of cells degrading CdvB highlighted in red is the same one plotted in the graph. Each blue spot represents a single cell, the density gradient going from blue to red, n = $10^6$.

Supplementary Figure 11 CdvB2 alone does not assemble into a division ring
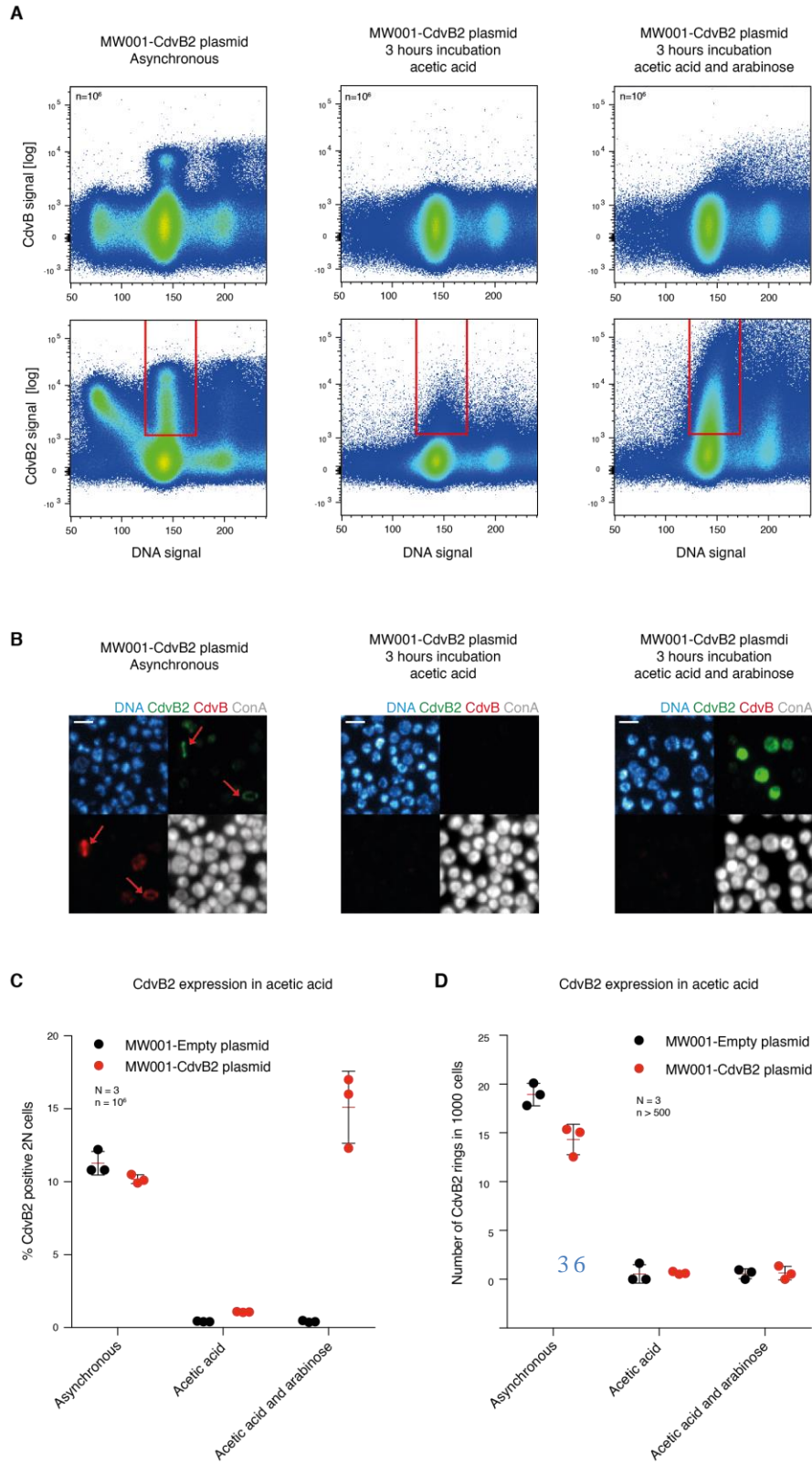
**Supplementary Figure 11 CdvB2 alone does not assemble into a division ring.** (**A**) Top, flow cytometry scatterplots with CdvB signal vs DNA signal for MW001 cells with an arabinose-inducible CdvB2 overexpression plasmid. Bottom, same as top, but for CdvB1 vs DNA signa. Left, the untreated asynchronous population. Middle, the population after three hours of acetic acid treatment. Right, the population after three hours of acetic acid and arabinose treatment. The red insert shows the CdvB2 positive cells in a 2N state. Each blue spot represents a single cell, the density gradient going from blue to red. Representative scatterplots shown, n = $10^6$. (**B**) unprocessed iSIM widefield microscopy images the cells under the three conditions stained for DNA, CdvB2, CdvB and ConA. The red arrows indicate division rings in the untreated asynchronous population. (**C**) Quantification of the percentage of 2N cells with high levels of CdvB2 in the three conditions. Error bars represent means ± SD from N = 3, n = $10^6$ (**D**) Quantification of the number of CdvB2 rings in 1000 in the three conditions. Error bars represent means ± SD from N = 3, n = $10^6$.

Supplementary Figure 12 Degradation of CdvB *in vitro*

**Supplementary Figure 12 In vitro degradation assay of CdvB by the 20S S. acidocaldarius proteasome in conditions with and without bortezomib.** (Lane 1) CdvB only control. (Lane 2) Using the inactive 20S proteasome (Saci_0613/Saci_0662ΔN) on the CdvB substrate. (Lane 3) Using the active 20S proteasome (Saci_0613/Saci_0662ΔN/Saci_0909ΔN) on the CdvB substrate in the absence of the bortezomib inhibitor. (Lane 4) As in Lane 3 but in the presence of 50 µM Bortezomib. (Lane 5) The active 20S proteasome alone as a no substrate control. Assays contained 30 µg of the 20S proteasomal complex incubated with 4 µg CdvB substrate for 120 minutes at 63°C. Two biological replicates shown. Blue arrows mark CdvB levels with the active proteasome in the absence of bortezomib. Conversely, red arrows mark the CdvB levels with the active proteasome in the presence of 50 uM bortezomib.

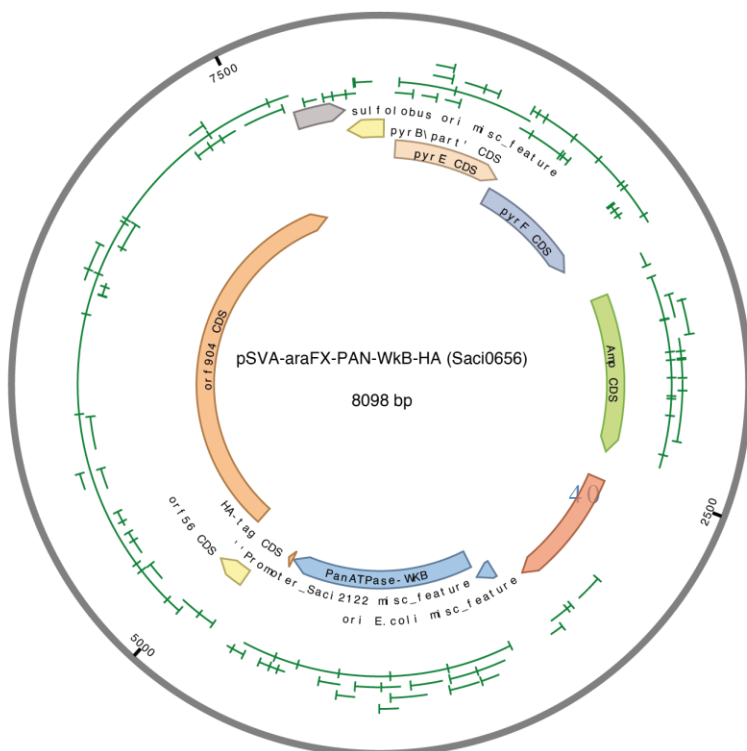Supplementary Figure 13 PAN-WalkerB-overexpression constructs

**A**

---

**Synthetic gene construct: PciI-Saci_0656-WkB-XhoI (PAN-WkB)**

gatagtacATGTTCGGGGATGTTGATAGTTATAAGAATCGTGAAAATAATAATAATTATGACGA
AACGCTTGTAAAACTTCTTGAAGAAAAAATAGAAGCTCTCACAAAAGAAATAGATAAATTA
AGACAAGATTTAAATTGGTATAAAACTGAACTAGAGAAACTACTGGCACCTCCATACATTG
AAGCTACAATATTAGATATATTACCAGACGGTAAGGTAATTGTAAGGAGCTCTTCGGGACC
AAACCTAGTTGTAAATGTAGCCACGAACGTCGATGTTTCCAAGTTAAAACCAGGCATGTC
TGTTGCATTAAGTCAAAGAGGATCAACGATTATAGATATTTTACCAAATAGAGAAGATATAA
TAGTAAAATCTTTTGAATTAATAGAGAAACCAAATATTCATTATTCTGATATAGGAGGTCTAG
AAGACCAGATAAACGAACTAAGAGAGGTAGTCGAATTACCATTAAAAAATAAGAAGTTATT
TGAAGAGCTAGGAATAGAGCCCCCTAAAGGAGTACTATTATATGGACCCCCTGGCACTG
GAAAAACCATGCTTGCCAAAGCTGTAGCAGCTGAAAGTAACGCCACATTTATTCATGTTG
TAGCATCAGAATTTGCCCAGAAATTTGTAGGAGAAGGGGCAAGAATAGTTAGAGAAGTC
TTTGAATTAGCTAGAAAGAAGGCTCCATCAATTAT**ATTCATAGATCAG**CTTGATGCGATTG
CTGCAAGAAGAATAGATATTGGTACAAGCGGTGAAAGGGAAATTCAAAGAACATTGATGC
AGTTATTGGCTGAAATTGATGGATTTAAGGCACTAGATAACGTTAAGATAATAGCAGCTAC
AAACAGAATCGACATATTAGATCCTGCTATACTAAGACCTGGTAGGTTTGATAGATTAATAG
AGGTTCCATTACCAGATGAGAAAGGTAGAAAGGAGATTTTCAAAATCTACCTCCAGAGAA
TGAGGATAAATGAAAACGATAAATTAAACTATGATCTAATTGCTCAACTCACAGACGGTTT
TAGTGGTGCAGACATTAAGAACGTTTGCACCGAAGCTGGATATATGGCCATAAGAGAAG
GAAGAGAGTCTATTAAATTCCAAGATATTATTAGAGCCATAGATAAAATAAAGAAAAAGAAT
TTAAGGAAAGCGATTAATACAAGAACCGAGAAATACTTACtcgaggatagt

---

**B**

**Supplementary Figure 13 PAN-WalkerB-overexpression constructs.** (**A**) The synthetic gene construct of PAN-WalkerB (uppercase) with the 5' PciI and 3' XhoI cut sites highlighted in red. The Walker B motif and mutation [E237Q] is highlighted in yellow. (**B**) Plasmid map of pSVA-araFX-PAN-WkB-HA, with genes highlighted.

Supplementary Figure 14 CdvB2-overexpression constructs

**A**

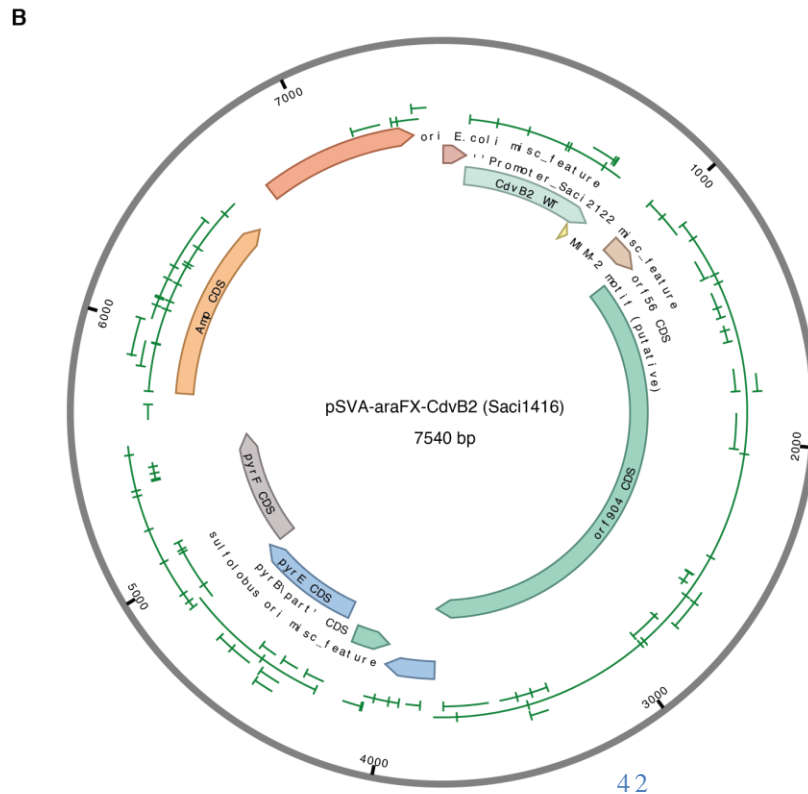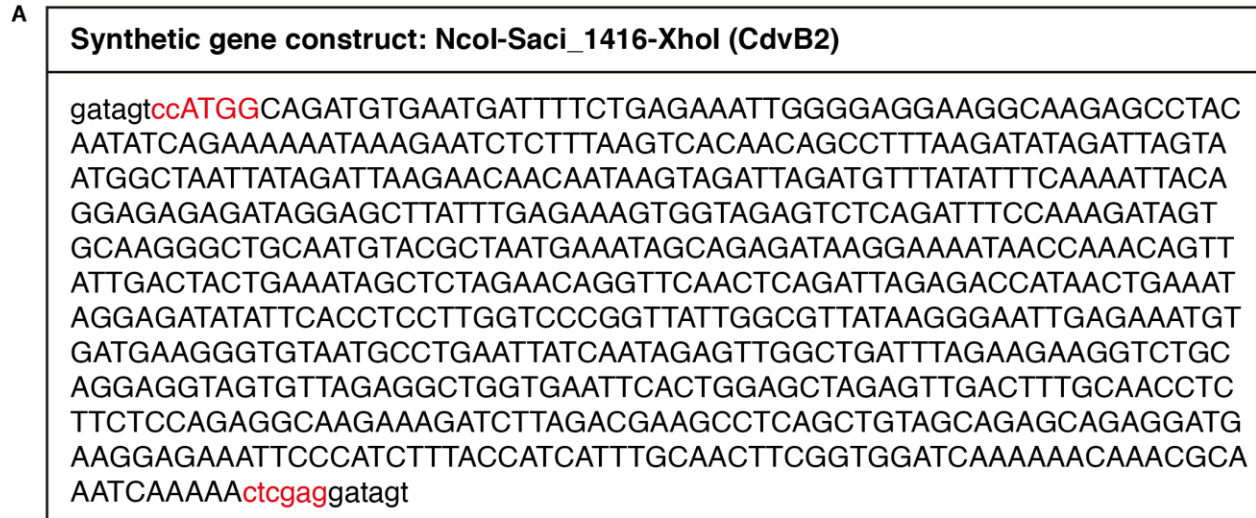| Synthetic gene construct: NcoI-Saci_1416-XhoI (CdvB2) |
|---|
| gatagtccATGGCAGATGTGAATGATTTTCTGAGAAATTGGGGGAGGAAGGCAAGAGCCTAC AATATCAGAAAAAATAAAGAATCTCTTTAAGTCACAACAGCCTTTAAGATATAGATTAGTA ATGGCTAATTATAGATTAAGAACAACAATAAGTAGATTAGATGTTTATATTTCAAAATTACA GGAGAGAGATAGGAGCTTATTTGAGAAAGTGGTAGAGTCTCAGATTTCCAAAGATAGT GCAAGGGCTGCAATGTACGCTAATGAAATAGCAGAGATAAGGAAAATAACCAAACAGTT ATTGACTACTGAAATAGCTCTAGAACAGGTTCAACTCAGATTAGAGACCATAACTGAAAT AGGAGATATATTCACCTCCTTGGTCCCGGTTATTGGCGTTATAAGGGAATTGAGAAATGT GATGAAGGGTGTAATGCCTGAATTATCAATAGAGTTGGCTGATTTAGAAGAAGGTCTGC AGGAGGTAGTGTTAGAGGCTGGTGAATTCACTGGAGCTAGAGTTGACTTTGCAACCTC TTCTCCAGAGGCAAGAAAGATCTTAGACGAAGCCTCAGCTGTAGCAGAGCAGAGGATG AAGGAGAAATTCCCATCTTTACCATCATTTGCAACTTCGGTGGATCAAAAAACAAACGCA AATCAAAAActcgaggatagt |

**B**



pSVA-araFX-CdvB2 (Saci1416)
7540 bp

42

**Supplementary Figure 14 CdvB2-overexpression constructs.** (**A**) The synthetic gene construct of CdvB2 (uppercase) with the 5' NcoI and 3' XhoI cut sites highlighted in red. (**B**) Plasmid map of pSVA-araFX-CdvB2, with genes highlighted.

**Supplementary Movie 1 Constriction simulation without filament disassembly**

<File added separately>

**Supplementary Movie 2 Constriction simulation with filament disassembly**

<File added separately>

**Supplementary Table 1 Data collection and refinement statistics for the Saci_0613/Saci_0662ΔN Proteasome**

**Data Collection**

| | |
|---|---|
| Space group | P 21 21 21 |

**Cell Dimensions**

| | |
|---|---|
| a, b, c (Å) | 108.289 193.654 323.671 |
| a, b, g (°) | 90 90 90 |
| Wavelength (Å) | 0.9801 |
| Resolution range (Å) | 48.19 - 3.698 (3.83 - 3.698) * |
| Mean I/sigma | 5.64 (1.56) |
| Completeness (%) | 99.21 (96.06) |
| Wilson B-factor | 82.08 |
| Multiplicity | 2.0 (2.0) |

**Refinement**

| | |
|---|---|
| Total reflections | 144662 (13665) |
| Unique reflections | 73138 (6972) |
| R-work | 0.2873 (0.3422) |
| R-free | 0.3343 (0.3992) |
| Reflections used in refinement | 73060 (6967) |
| Reflections used for R-free | 3676 (347) |
| Number of non-hydrogen atoms | 41436 |
| Macromolecules | 41436 |
| Protein residues | 5391 |
| RMS (bonds) | 0.002 |
| RMS (angles) | 0.57 |
| Ramachandran favoured (%) | 94.7 |
| Ramachandran allowed (%) | 4.96 |
| Ramachandran outliers (%) | 0.34 |
| Rotamer outliers (%) | 0.61 |
| Clashscore | 11.63 |
| Average B-factor | 76.94 |

*Statistics for the highest-resolution shell are shown in parenthesis

**Supplementary Table 2 Mass spectrometry tables with Cdv proteins**

(**A**)

|  | CdvA | CdvB | CdvC | CdvB1 | CdvB2 |
|---|---|---|---|---|---|
| **Experiment 1**<br>Log2 [bortezomib] - Log2 [bortezomib wash-out] | 0.36 | 2.53 | -0.07 | -0.44 | 0.32 |
| **Experiment 2**<br>Log2 [bortezomib] - Log2 [bortezomib wash-out] | 0.26 | 2.84 | 0.54 | 1.03 | 0.53 |
| **Experiment 3**<br>Log2 [bortezomib] - Log2 [bortezomib wash-out] | -0.40 | 2.44 | -0.08 | -0.14 | 0.11 |

(**B**)

|  | CdvA | CdvB | CdvC | CdvB1 | CdvB2 |
|---|---|---|---|---|---|
| **Experiment 1**<br>Log2 [MG132] - Log2 [DMSO] | -0.30 | 1.44 | -1.08 | -0.26 | -0.25 |
| **Experiment 2**<br>Log2 [MG132] - Log2 [DMSO] | -0.45 | 4.53 | 1.51 | -0.04 | -0.58 |
| **Experiment 3**<br>Log2 [MG132] - Log2 [DMSO] | 0.34 | 2.72 | 0.89 | 0.67 | 0.07 |

**Supplementary Table 3 List of antibody host species and secondary antibodies**

| Target | Primary antibody host | Secondary antibody |
|---|---|---|
| **CdvB** | Rabbit | Goat anti-Rabbit AlexaFluor 546 (Invitrogen, A11035) |
| **CdvB1** | Chicken | Goat anti-Chicken AlexaFluor 488 (Invitrogen, A11039) |
| **CdvB1** | Chicken | Goat anti-Chicken AlexaFluor 555 (Invitrogen, A21437) |
| **CdvB2** | Guinea Pig | Goat anti-Rabbit AlexaFluor 546 (Invitrogen, A11073) |

**Supplementary Table 4 List of primers used in cloning of plasmids used for protein expression**

| Gene | Sequence |
|------|----------|
| cdvB-F Saci_1373 | GATATTATTGAGGCTCACAGAGAACAGATTGGTGGGATGTTTGATAAGTTATCGATAATTTT |
| cdvB-R Saci_1373 | GCAGCCGGATCTCAGTGGTGGTGGTGGTGGTGCTCGAGTTAACCCTCAAGAACAATTAGAC |
| cdvB1-F Saci_0451 | GATATTATTGAGGCTCACAGAGAACAGATTGGTGGGATGACCGCAATATATATATTGACC |
| cdvB1-R Saci_0451 | GCAGCCGGATCTCAGTGGTGGTGGTGGTGGTGCTCGAGTTAGCTCTTTTGTTGCTGTGTAA |
| cdvB2-F Saci_1416 | GATATTATTGAGGCTCACAGAGAACAGATTGGTGGGATGGCAGATGTGAATGATTTTCTGAG |
| cdvB2-R Saci_1416 | GCAGCCGGATCTCAGTGGTGGTGGTGGTGGTGCTCGAGTTATTTTTGATTTGCGTTTGTTTTTT |

**Supplementary Table 5 List of primers used for RT-qPCR analysis**

| *Saci annotation* | Gene | Sequence |
|---|---|---|
| Forward Saci_0574 | *secY* | ACTCTTGCTTGACGAGATGATAC |
| Reverse Saci_0574 | *secY* | ACTCTGTACGGAGACTATTCCA |
| Forward Saci_1374 | *cdvA* | GGACAGATGGAGAAGATAAGGAAG |
| Reverse Saci_1374 | *cdvA* | TGAGCAACTTGGTCCTCTATTG |
| Forward Saci_1373 | *cdvB* | ACTGGTGCATTAAGCGAGAA |
| Reverse Saci_1373 | *cdvB* | TTGGTAACTCTGAAGGTGGATG |
| Forward Saci_1372 | *cdvC* | GCTGTAGCTAATGAGATCGACTCATATT |
| Reverse Saci_1372 | *cdvC* | CAGCCTCGCCTAGCCACTTA |
| Forward Saci_0451 | *cdvB1* | GGTGAACTAGGTGAAGGTTTACA |
| Reverse Saci_0451 | *cdvB1* | CTGTCTTGCCTCTGGTGAATAG |
| Forward Saci_1416 | *cdvB2* | CTCTTCTCCAGAGGCAAGAAAG |
| Reverse Saci_1416 | *cdvB2* | CCGAAGTTGCAAATGATGGTAAA |